Journal of Applied Physics

Effects of vacancies on luminescence of Er-doped $0.93Bi_{0.5}Na_{0.5}TiO_3$-$0.07BaTiO_3$ ceramics

Cite as: J. Appl. Phys. **118**, 034107 (2015); https://doi.org/10.1063/1.4927297
Submitted: 13 May 2015 . Accepted: 12 July 2015 . Published Online: 21 July 2015

Chi Man Lau, Xiao Wu, and K. W. Kwok

Effects of vacancies on luminescence of Er-doped $0.93Bi_{0.5}Na_{0.5}TiO_3$-$0.07BaTiO_3$ ceramics

Chi Man Lau, Xiao Wu, and K. W. Kwok[a)]
Department of Applied Physics and Materials Research Centre, The Hong Kong Polytechnic University, Kowloon, Hong Kong, China

(Received 13 May 2015; accepted 12 July 2015; published online 21 July 2015)

$0.93Bi_{0.5}Na_{0.5}TiO_3$-$0.07BaTiO_3$ ceramics doped with 0.01 mol Er^{3+} have been prepared and their photoluminescence (PL), ferroelectric, dielectric, and piezoelectric properties have been studied. By doping Er^{3+} at various sites, ceramics containing oxygen or cation vacancies have been prepared and their effects have been investigated. Ceramic containing no vacancy (i.e., doping Er^{3+} at the Bi^{3+} site) has also been prepared as a reference for the study. In addition to the reduction of the up-conversion PL emissions at 532, 547, and 660 nm, our results also reveal that oxygen vacancies can enhance, at the expense of the visible emissions, the near-infrared (1.44–1.66 μm) and mid-infrared (2.62–2.84 μm) down-conversion emissions. Similar results have also been observed for the ceramics containing cation vacancies, and the enhancement in the near-infrared emission becomes much more significant, reaching about 70% for the ceramic doped with Er^{3+} at the Na^{+} site. These should be attributed to the looping mechanism between the $^4F_{7/2}$, $^2H_{11/2}$, $^4I_{9/2}$, and $^4I_{11/2}$ levels facilitated by the cation vacancies and the efficient cross relaxations. The ceramics also exhibit reasonably good ferroelectric, dielectric, and piezoelectric properties, suggesting that they have great potential for multifunctional applications. © *2015 AIP Publishing LLC*. [http://dx.doi.org/10.1063/1.4927297]

I. INTRODUCTION

Owing to the wide emission range (from ultraviolet (UV) to near-infrared (NIR)) and high conversion efficiency in up-conversion (UC) and down-conversion (DC) luminescent emissions, trivalent rare-earth ions (RE^{3+}) have been extensively investigated as luminescent centers or activators in RE^{3+}-doped luminescent materials for applications in solid state lasers, biological imaging, spectral convertor, optical telecommunication, military countermeasures, remote sensing, atmospheric pollution monitoring, and optical parametric oscillators.[1–6] It has been reported that Er^{3+}, Tm^{3+}, and Ho^{3+} can exhibit efficient UC and DC luminescent emissions in the visible (Vis) and IR regions, respectively.[1] The long lifetime (1–20 ms) of the metastable states of RE^{3+} has been shown to be an important factor for the efficient UC processes.[2,3]

Lead zirconia titanate-based piezoelectric ceramics have been widely used for sensors,[7] ultrasonic transducers,[8] and actuators[9] because of their excellent piezoelectric properties. However, due to the increasing concern of lead-pollution, the research of lead-free piezoelectric materials for replacing lead-containing piezoelectric materials has attracted considerable attention recently. Among various lead-free candidates, $Bi_{0.5}Na_{0.5}TiO_3$ (BNT) is one of the most promising lead-free candidates, which has been studied extensively. It exhibits a high Curie temperature (T_c = 320 °C) and strong ferroelectricity (remanent polarization $P_r = 38\ \mu C/cm^2$).[11] However, it has a high conductivity and coercive field ($E_c = 7.3$ kV/mm), which cause the poling extremely difficult and then poor piezoelectric properties (piezoelectric coefficient $d_{33} = 73$–80 pC/N).[12] A number of BNT-based solid solutions have been developed for improving the poling process and enhancing the piezoelectric properties. $(1-x)Bi_{0.5}Na_{0.5}TiO_3$-$xBaTiO_3$ is one of those solid solutions which possesses a morphotropic phase boundary (MPB) at x = 0.06–0.07. Similar to the other perovskite systems, the composition near the MPB exhibits an enhanced d_{33} (155 pC/N) and electromechanical coupling coefficient ($k_p = 36.7\%$).[11] Recently, there are numerous research works on developing new multifunctional materials that possess both the photoluminescence (PL) and ferroelectric properties. It has been shown that, in addition to good piezoelectric and PL properties, Er/Yb co-doped BNT ceramics also exhibit temperature-dependent PL emissions, which is promising for optical temperature sensing applications.[13] The effects of oxygen vacancies (V_o) on PL properties have also been extensively investigated. As V_o can trap electrons in higher energy levels and then terminate the PL emissions via non-radiative transitions, the PL properties of luminescent materials containing V_o are commonly deteriorated.[14–16] However, most of the research works have focused on the Vis PL emissions and seldom on the IR emissions. There is also little work studying the effects of cation vacancies (V_c).

In this work, $0.93Bi_{0.5}Na_{0.5}TiO_3$–$0.07BaTiO_3$ (BNBT) ceramics doped with 0.01 mol Er^{3+} at various sites, i.e., $0.93(Bi_{0.5-x/0.93}Er_{x/0.93}Na_{0.5})TiO_3$−$0.07BaTiO_3$, $0.93(Bi_{0.5}Na_{0.5-3x/0.93}Er_{x/0.93})TiO_3$–$0.07BaTiO_3$, $0.93Bi_{0.5}Na_{0.5}(Ti_{1-x/0.93}Er_{x/0.93})O_{3-0.5x/0.93}$–$0.07BaTiO_3$, and $0.93Bi_{0.5}Na_{0.5}TiO_3$–$0.07(Ba_{1-1.5x/0.07}Er_{x/0.07})TiO_3$, have been fabricated, and the effects of the resulting vacancies (V_o or V_c) on PL properties have been investigated. The ceramic samples are abbreviated as

a)Author to whom correspondence should be addressed. Tel.: +852 27665667. Fax: +852 23337629. Electronic mail: apkwkwok@polyu.edu.hk

BNBT-Er(y), where y is Bi, Na, Ti, or Ba for denoting the ions being replaced by Er^{3+}. Depending on the charge difference between Er^{3+} and the ions being replaced, either V_o or V_c will be formed for retaining the charge neutrality.[17] V_o is formed in the BNBT-Er(Ti) ceramics, whereas V_c is formed in the ceramics with y = Ba and Na. Owing to the different valence states (+2 vs +1), the number of V_c in the BNBT-Er(Ba) ceramic should be about half of that in BNBT-Er(Na). On the other hand, because of the same valence state of Er^{3+} and Bi^{3+}, no vacancies will be formed in the BNBT-Er(Bi) ceramics. The PL emissions, including NIR and mid-IR (MIR) DC emissions, as well as Vis UC emissions, have been studied, and the corresponding PL mechanisms and energy transfer (ET) processes have been deduced. The ferroelectric, dielectric, and piezoelectric properties have also been evaluated for demonstrating the multi-functionality of the BNBT-Er(y) ceramics.

II. EXPERIMENT

The BNBT-Er(y) ceramics were prepared by a conventional ceramic fabrication technique using analytical-grade metal oxides or carbonates powders: Bi_2O_3 (99.9%), Na_2CO_3 (99%), $BaCO_3$ (99.5%), TiO_2 (99.9%), and Er_2O_3 (99.99%). Un-doped BNBT, i.e., BNBT-Er(0), ceramic has also been fabricated for comparison purposes. The powders in the stoichiometric ratio of the compositions were mixed thoroughly in ethanol using zirconia balls for 8 h, and calcined at 850 °C for 2 h. The calcined powders were then ball-milled again for 8 h and mixed thoroughly with a 5-wt. % polyvinyl alcohol binder solution, and pressed into disk samples with a diameter of 12 mm. The disk samples were sintered at 1200 °C for 2 h in air. Silver electrodes were fired on the top and bottom surfaces of the sintered samples at 750 °C for 30 min for the subsequent poling and electrical measurements. The samples were poled under a dc field of 5 kV/mm at 60 °C in a silicone oil bath for 20 min.

The crystallite structure of the sintered ceramics was examined using X-ray diffraction (XRD) analysis with CuK_α radiation (Smartlab, Rigaku Co., Tokyo, Japan), and the microstructure was observed using a field-emission scanning electron microscope (FE-SEM) (JSM-6335 F JEOL, Tokyo, Japan). The average grain size was determined by the measurement of 250 grains on SEM micrographs using the linear intercept method with a correction factor of 1.56. A conventional Sawyer-Tower circuit was used to measure the polarization hysteresis (P-E) loop at 10 Hz. The room-temperature dielectric constant ε_r and dielectric loss $\tan\delta$ at 1 kHz were measured using an impedance analyzer (HP 4294 A, Agilent Technologies, Inc., Palo Alto, CA). The piezoelectric coefficient d_{33} was measured using a piezo-d_{33} meter (ZJ-3A, China).

The Raman spectrum was measured in backscattering geometry using the 488-nm line of an Ar ion laser (Spectra-Physics) as the excitation source. The spectrum was recorded using a grating spectrometer (Horiba, Jobin-Yvon HR800, France). The PL emission spectrum was measured using a spectrophotometer (FLSP920, Edinburgh Instruments, UK). A 980-nm diode laser (MDL-III, CNI Optoelectronics Tech. Co., China) with a maximum power of 2 W was used to generate excitation source (continuous waves) for the measurements of Vis (450–700 nm) UC luminescence as well as NIR (1.40–1.70 μm) and MIR (2.60–2.90 μm) DC luminescence. The diode laser was also used to generate pulsed signals, by using an external Transistor-Transistor Logic (TTL) signal with a repetition rate of 100 H and duty circle of 10% produced by a function generator (AFG3251, Tektronix, USA), as the excitation source for the decay curve measurement. All the spectroscopic measurements were conducted at room temperature, and all the ceramic specimens were thinned to the same thickness.

III. RESULTS AND DISCUSSION

The XRD patterns of the BNBT-Er(y) ceramics, in crushed powder form, are shown in Fig. 1. All the ceramics possess a perovskite structure and no secondary phase is observed, suggesting that Er^{3+} has diffused into and entered the corresponding sites of the BNBT lattices. Similar to the un-doped BNBT ceramic,[10,18] all the ceramics exhibit a splitting of the (002)/(200) diffraction peaks (Fig. 1(b)), confirming that all of them reside near the MPB and contain both the rhombohedral and tetragonal phases. As also shown in Fig. 1(b), the diffraction peaks of the ceramics with y = Bi, Ba, and Na shift slightly towards higher angles. These should be attributed to the smaller ionic radius of Er^{3+} (1.22 Å, CN = 12)[19] as compared to the A-site Bi^{3+} (1.32 Å), Ba^{2+} (1.61 Å), and Na^+ (1.39 Å). Probably due to the low Er-concentration (0.01 mol) and possible lattice distortions arisen from the cation vacancies, the peak shifting is insignificant. On the other hand, as Er^{3+} is larger than the B-Site Ti^{4+} (0.605 Å vs 0.89 Å, CN = 6), the diffraction peaks of the BNBT-Er(Ti) ceramic shift slightly to lower angles.

The FE-SEM micrographs of the BNBT-Er(y) ceramics are shown in Fig. 2, and their average grain sizes are listed in Table I. All the ceramics possess a well-sintered and dense structure. As shown in Table I, the average grain size decreases from 1.07 to 0.90–0.84 μm (or by 16 to 21%) after the doping of Er^{3+}. This should be attributed to the inhibition of grain growth caused by the Er-doping.[20] It can be seen that the grains are not uniform in size. Similar to the previous

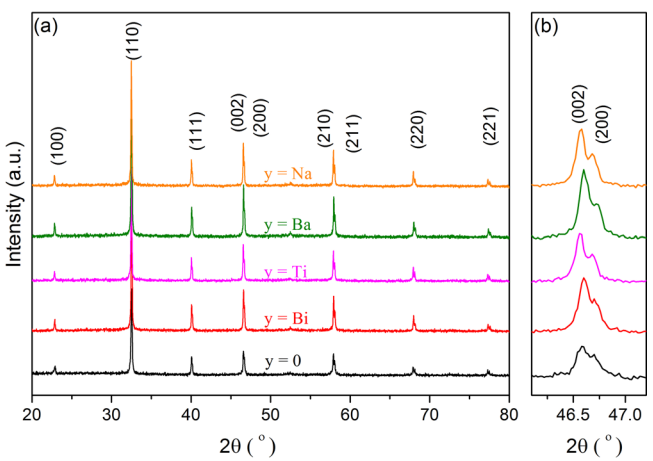

FIG. 1. XRD patterns of the BNBT-Er(y) ceramics.

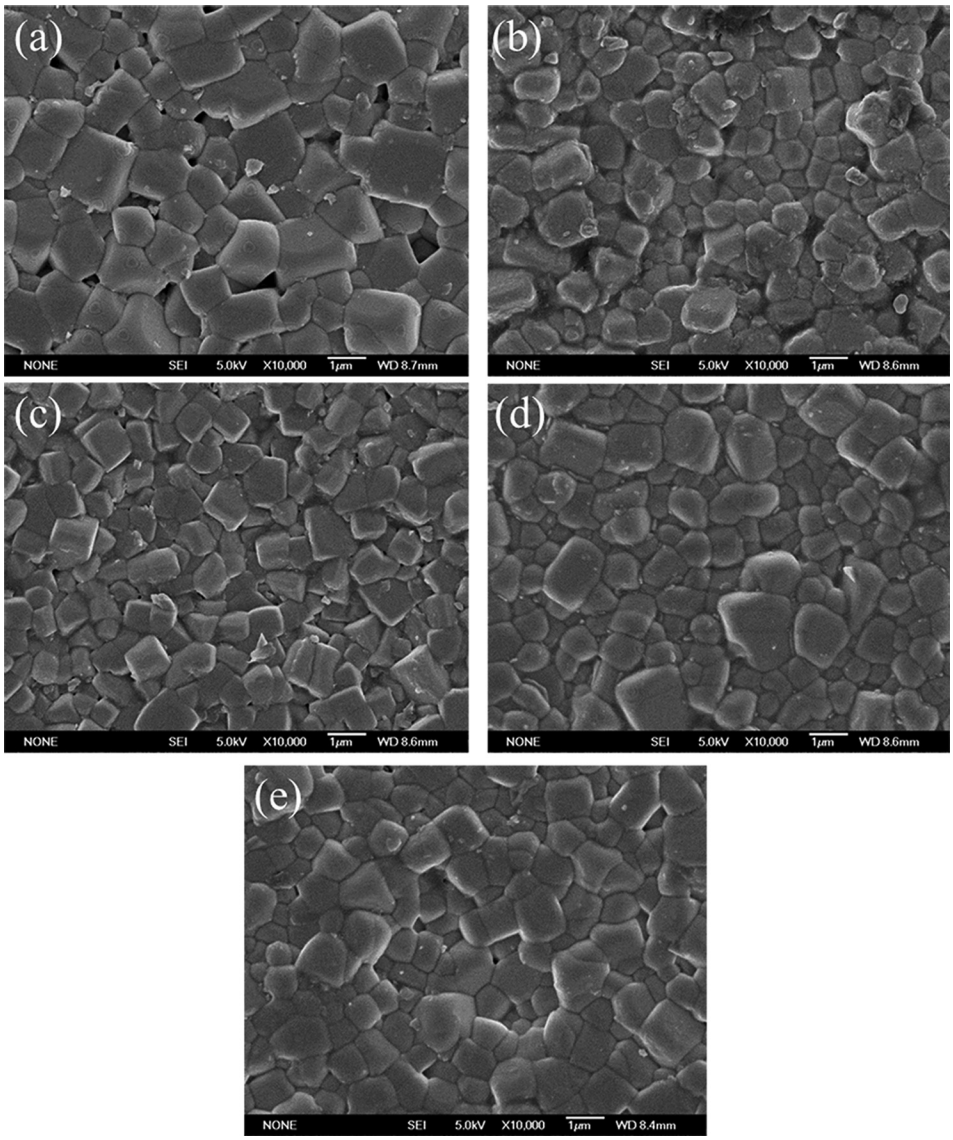

FIG. 2. FE-SEM micrographs of the BNBT-Er(y) ceramics: (a) y = 0, (b) y = Bi, (c) y = Ti, (d) y = Ba, and (e) y = Na.

works on Dy-doped BT and BNT ceramics, the non-uniformity may be attributed to the various sizes of the starting powders that have different priorities in the sintering process.[21,22]

The Raman spectra of the BNBT-Er(y) ceramics and the fitting curves for the BNBT-Er(0) ceramic are shown in Fig. 3. Consistent with the previous results of BNBT,[12] five Raman-active modes relating to various vibrations of the octahedral [BiO_6], [NaO_6], and [TiO_6] (undistorted or distorted) clusters were observed in the range of 100 to 1000 cm^{-1} for all the ceramics. As revealed by the fitting cures for the BNBT-Er(0) ceramic, one of the modes should locate at ~240 cm^{-1}. Because of the dependence on the short-range electrostatic forces of the lattice iconicity, this mode is generally weak and barely observable in the spectra. The mode located at ~600 cm^{-1} is related to the stretching

TABLE I. Physical properties of the BNBT-Er(y) ceramics.

Y	Grain size (μm)	P_r ($\mu C/cm^2$)	ε_r	tanδ	d_{33} (pC/N)
0	1.07	31	1813	0.057	194
Bi	0.87	16	1616	0.050	27
Ti	0.84	8.1	1564	0.048	26
Ba	0.84	9.2	1485	0.045	13
Na	0.90	5.1	1596	0.049	8

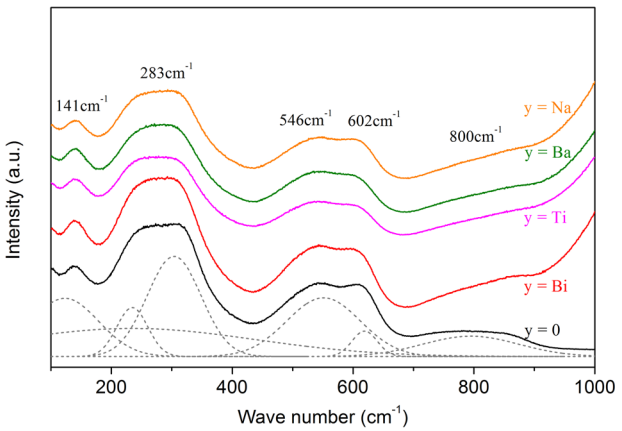

FIG. 3. Raman spectra of the BNBT-Er(y) ceramics. The fitting curves for the BNBT-Er(0) ceramics are shown as dotted lines for identifying the Raman-active modes.

symmetric vibrations of the [TiO_6] clusters. The splitting into two bands at ~546 cm^{-1} and ~602 cm^{-1} should be attributed to the coexistence of the rhombohedral and tetragonal phases, and thus confirming the MPB composition of the ceramics (Fig. 1). As also shown in Fig. 3, the peaks of the ceramics with y = Ti, Ba, and Na are broadened. This should be attributed to the vacancies (V_o or V_c), which act as defects to deteriorate the crystallinity of the ceramics.[15] The largest peak broadening observed for the BNBT-Er(Na) ceramic suggests that it should contain more V_c.

The Vis UC PL emission spectra of the BNBT-Er(y) ceramics are shown in Fig. 4, while the NIR and MIR DC emission spectra are shown in Figs. 5 and 6, respectively. Under an excitation of 980 nm, the visible emission of the ceramics is very strong and a bright green spot on the irradiated surface can be easily observed by the naked eye during the measurement. As shown in Fig. 4, all the BNBT-Er(y) ceramics exhibit three characteristic emission bands at 512–536 nm (green), 536–569 nm (green), and 640–681 nm (red), respectively. They are attributed to the transitions $^2H_{11/2} \rightarrow {}^4I_{15/2}$, $^4S_{3/2} \rightarrow {}^4I_{15/2}$, and $^4F_{9/2} \rightarrow {}^4I_{15/2}$, respectively (Fig. 7). On the other hand, attributing to the transitions $^4I_{13/2} \rightarrow {}^4I_{15/2}$ and $^4I_{11/2} \rightarrow {}^4I_{13/2}$ of Er^{3+} (Fig. 7), all the ceramics exhibit a broad NIR and MIR emission bands, respectively, in the range of 1.44–1.66 μm (Fig. 5) and 2.62–2.84 μm (Fig. 6).

As illustrated in the simplified energy level diagram of Er^{3+} (Fig. 7), electrons are first excited by the 980-nm photons to the $^4I_{11/2}$ level through ground state absorption (GSA). Some of them may further be excited to the $^4F_{7/2}$ level through excited state absorption (ESA1). The excited electrons will relax non-radiatively to the $^2H_{11/2}$, $^4S_{3/2}$, and $^4F_{9/2}$ levels, respectively, by multi-phonon relaxation (MPR) and then relax radiatively to the $^4I_{15/2}$ ground level, producing the green and red UC emissions as shown in Fig. 4. Probably due to the small energy gap between the $^2H_{11/2}$ and $^4S_{3/2}$ levels, the MPR rate for the transition $^2H_{11/2} \rightarrow {}^4S_{3/2}$ is fast, and thus resulting in the low population of the $^2H_{11/2}$ level and the weak emission at 532 nm. On the other hand, due to the large energy gap between the $^4S_{3/2}$ and $^4F_{9/2}$ levels and then the slow MPR rate, the population of the $^4F_{9/2}$ level

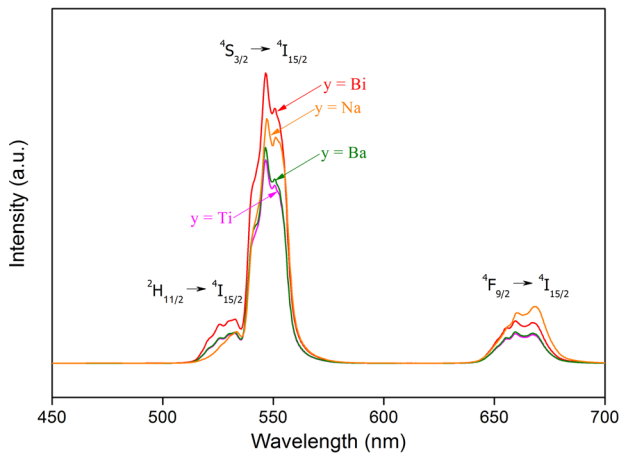

FIG. 4. Visible up-conversion PL emission spectra of the BNBT-Er(y) ceramics.

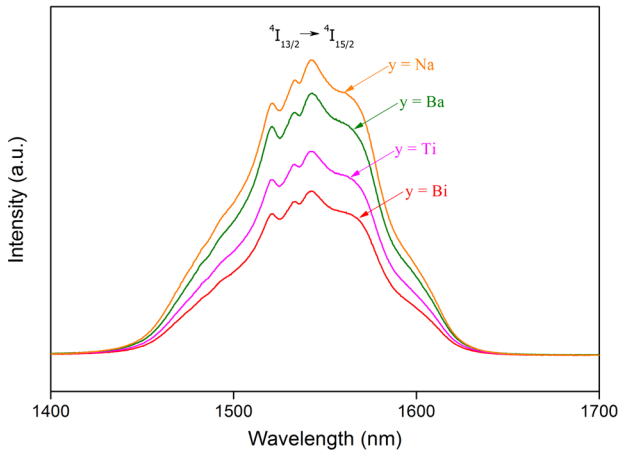

FIG. 5. NIR down-conversion PL emission spectra of the BNBT-Er(y) ceramics.

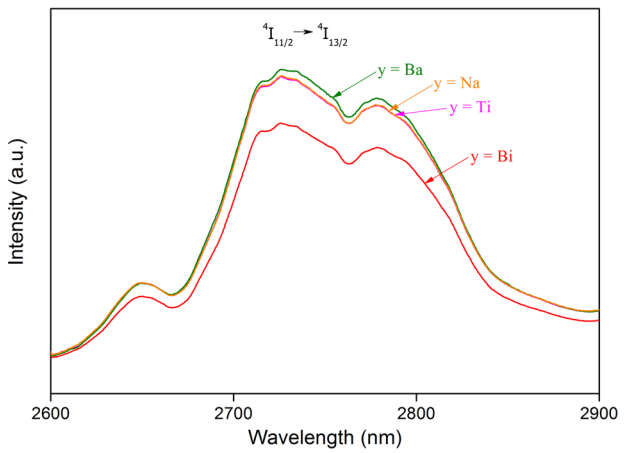

FIG. 6. MIR down-conversion PL emission spectra of the BNBT-Er(y) ceramics.

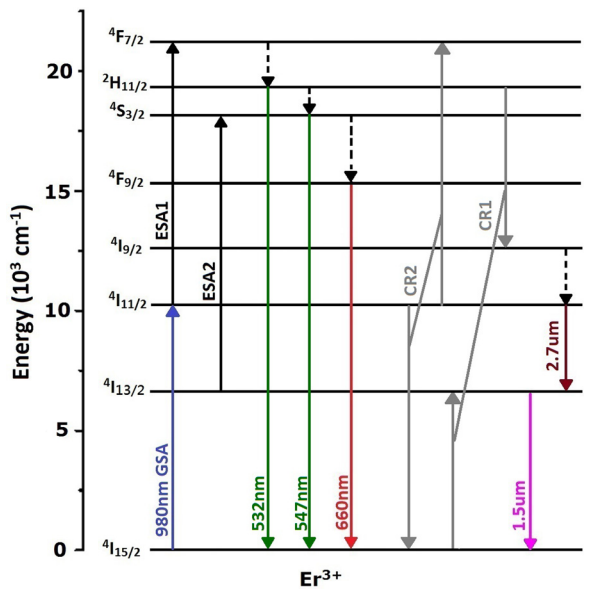

FIG. 7. Schematic diagram for the PL mechanism of Er^{3+} under an excitation of 980 nm.

is low and the red emission is weak (Fig. 4). The $^4F_{9/2}$ level can also be populated by a cross relaxation process ($^4I_{15/2} + {}^2H_{11/2} \rightarrow {}^4I_{13/2} + {}^4I_{9/2}$) followed by an energy transfer process ($^4I_{13/2} \rightarrow {}^4F_{9/2}$),[xx] or directly by a cross relaxation process ($^4F_{7/2} + {}^4I_{11/2} \rightarrow {}^4F_{9/2}$).[23] However, it has been shown that the cross relaxation processes become efficient only at high Er-concentrations (e.g., $\geq$0.02 mol).[24] At low concentrations, the electrons in the $^4I_{11/2}$ level will have higher probability to relax radiatively to the $^4I_{13/2}$ level and then to the $^4I_{15/2}$ ground level (Fig. 7), producing the NIR and MIR DC emissions, respectively, as shown in Figs. 5 and 6.

The relative integrated PL intensities of the green (507–580 nm), red (635–695 nm), NIR (1.44–1.66 μm), and MIR (2.62–2.84 μm) emission bands of the BNBT-Er(y) ceramics are shown in Fig. 8. As the BNBT-Er(Bi) ceramic contains no vacancies, it is chosen as a reference for the study. As discussed in Section I, due to the different valence states, the BNBT-Er(Ti) ceramic should contain oxygen vacancies V_o, while the BNBT-Er(Ba) and BNBT-Er(Na) ceramics should contain cation vacancies V_c.[17] Moreover, the BNBT-Er(Ti) and BNBT-Er(Ba) ceramics should contain similar amounts of vacancies (V_o or V_c), whereas the amount of V_c in the BNBT-Er(Ba) ceramic should be about half of that in BNBT-Er(Na). As shown in Fig. 8, the observed PL intensities of the green and red emission bands for the ceramics containing V_c or V_o generally become smaller, whereas those of the NIR and MIR emission bands become larger.

It has been shown that the (visible) luminescence of Er^{3+} and Pr^{3+} can be quenched by a small amount of V_o.[19,25] Similarly, owing to the positive charge, V_o acts as a trap for the excited electrons in the $^4F_{7/2}$ level of the BNBT-Er(Ti) ceramic. As a result, the populations of the $^2H_{11/2}$, $^4S_{3/2}$, and $^4F_{9/2}$ levels become lower and the corresponding visible emissions become weaker. On the other hand, the energy level of V_o has been shown to be $\sim$10 000 cm^{-1} below the bottom of the conduction band of $SrTiO_3$.[26] Parija *et al.* have shown that the bandgap of BNT ceramics is 2.94 eV.[27] The energy level of V_o in the BNBT-Er(Ti) ceramic should then reside above the $^4I_{11/2}$ level of Er^{3+}. As a result, the population of the $^4I_{11/2}$ level may be increased by the electrons relaxed non-radiatively from V_o, and thus enhancing the NIR and MIR emissions as shown in Fig. 8.

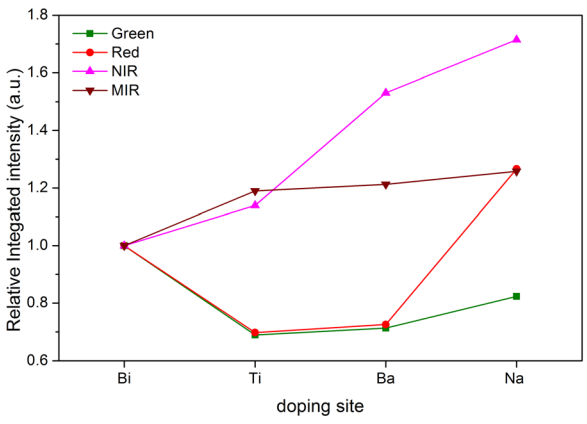

FIG. 8. Relative integrated intensities of the green, red, NIR, and MIR PL emissions of the BNBT-Er(y) ceramics.

On the other hand, V_c is regarded as a non-radiative recombination center (NRCs),[28,29] which increases the probabilities of cross relaxations CR1 ($^4I_{15/2} + {}^2H_{11/2} \rightarrow {}^4I_{13/2} + {}^4I_{9/2}$) and CR2 ($^4I_{11/2} \rightarrow {}^4I_{15/2} + {}^4F_{7/2}$) and thus facilitates a looping mechanism between the $^4F_{7/2}$, $^2H_{11/2}$, $^4I_{9/2}$, and $^4I_{11/2}$ levels for the BNBT-Er(Ba) and BNBT-Er(Na) ceramics (Fig. 7). As a result, the population of the $^4H_{11/2}$ level become lower, and all the visible emissions are weakened. On the other hand, the populations of the $^4I_{11/2}$ and $^4I_{13/2}$ levels are increased subsequently, and thus enhancing the NIR and MIR emissions. As also illustrated in Fig. 7, the $^4I_{13/2}$ level is populated by electrons both excited from the $^5I_{15/2}$ ground level (via CR1) and relaxed from the $^4I_{11/2}$ level. The enhancement for the NIR emission then becomes much more significant, reaching more than 70% for the BNBT-Er(Na) ceramic. Apparently, the effects (including both the decreases in the PL intensities of visible emissions and increases in that of NIR and MIR emissions) should be proportional to the amount of V_c. However, increases in the observed PL intensities of the visible emissions are observed for the BNBT-Er(Na) ceramic (which should contain more V_c) (Fig. 8). These should be attributed to another excited state absorption ESA2 as shown in Fig. 7. Owing to the increased population of the $^4I_{13/2}$ level, some of the excited electrons may further be excited to the $^4S_{3/2}$ level via ESA2.[30] Probably due to the enhanced MPR (resulted from more V_c), most of them will not relax radiatively to give green emission. Instead, they will relax non-radiatively to the $^4F_{9/2}$ level and then radiatively to the $^4I_{15/2}$ ground level, giving an enhancement in the red emission. Although the red emission of all the ceramics are weak (as compared with the green emission), it is noted that the red emission of the BNBT-Er(Na) ceramic (with more V_c) is even stronger than that of the BNBT-Er(Bi) ceramic.

The decay curves of the UC PL emissions at 547 nm ($^4S_{3/2} \rightarrow {}^4I_{15/2}$) and 660 nm ($^4F_{9/2} \rightarrow {}^4I_{15/2}$) for the BNBT-Er(y) ceramics are shown in Fig. 9. In general, the ceramics containing vacancies exhibit a shorter lifetime. It has been known that the lifetime can be reduced by V_o.[15] For the ceramics containing V_c, the reduction of lifetime may be attributed to the enhanced CRs that decrease the populations of the $^4S_{3/2}$ and $^4F_{9/2}$ levels. Chai *et al.* have reported similar results that the lifetime of the $^4I_{13/2}$ and $^4I_{11/2}$ levels of Er^{3+}-doped YF_3/YOF crystals is decreased by the enhanced ET processes.[30] However, probably due to the larger population, the lifetime of the $^4F_{9/2}$ level for the BNBT-Er(Na) ceramic is longer than that for the BNBT-Er(Bi) ceramic.

The P-E loops of the BNBT-Er(y) ceramics measured under an electric field of 5.5 kV/mm at 100 Hz are shown in Fig. 10. After the doping of Er^{3+}, the P-E loop becomes slanted, showing a decrease in the remanent polarization (P_r). The deterioration of ferroelectric properties should be attributed to the disruption of the long-range ferroelectric order by Er^{3+}.[31] The observed P_r as well as ε_r, tan δ, and d_{33} of the ceramics are listed in Table I. Both the observed ε_r and tan δ decrease after the doping of Er^{3+}, and the effects are not significantly dependent on the type and content of the vacancies. According to the phenomenological theory, d_{33} is

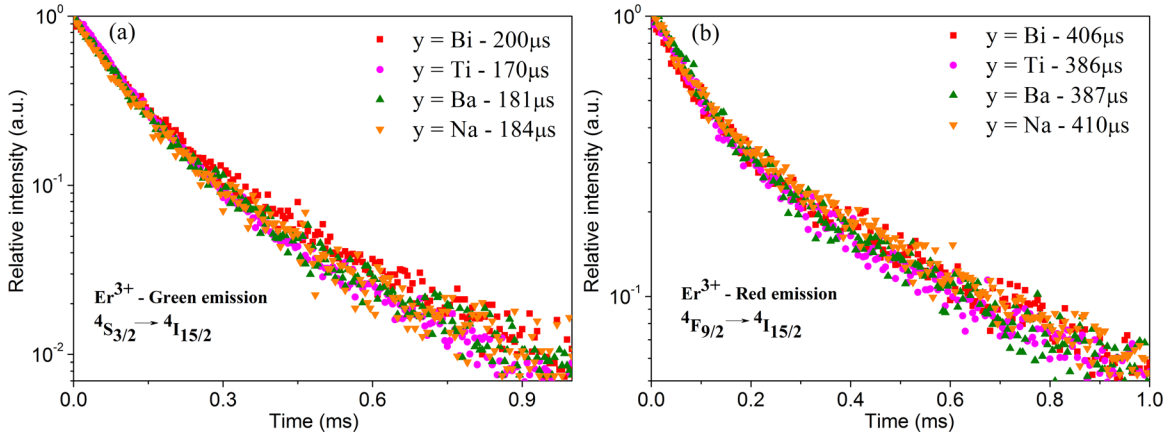

FIG. 9. Decay curves of the up-conversion PL emissions originating from different energy levels of Er^{3+}: (a) green emission at 547 nm ($^4S_{3/2} \rightarrow {}^4I_{15/2}$) and (b) red emissions at 660 nm ($^4F_{9/2} \rightarrow {}^4I_{15/2}$).

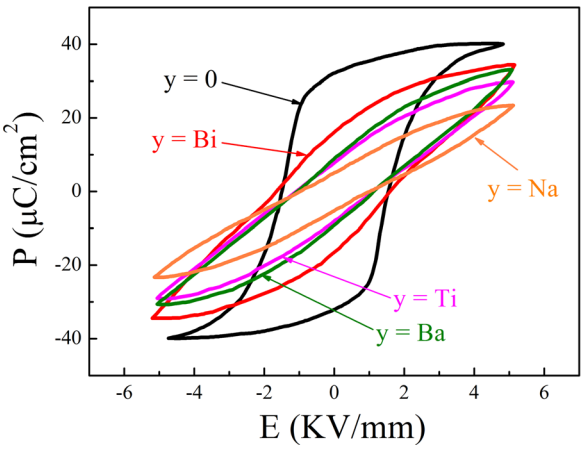

FIG. 10. P-E loops of the BNBT-Er(y) ceramics.

related to ε_r, the permittivity of vacuum ε_o, the spontaneous polarization P_s (which may be approximated by P_r), and the electrostrictive coefficient Q_{11} via a general equation $d33 = 2\varepsilon_o\varepsilon_r Q_{11}Ps$.[31] The significant decrease in d_{33} of the doped ceramics should hence be attributed partly to the decreases in both ε_r and P_r, and partly to the disruption of the long-range ferroelectric order.[31]

IV. CONCLUSIONS

BNBT-Er(y) photoluminescent ceramics have been fabricated, and their PL, ferroelectric, dielectric, and piezoelectric properties have been studied. All the ceramics possess a single-phase perovskite structure, suggesting that Er^{3+} has diffused into the corresponding sites of the BNBT ceramics successfully. Under an excitation of 980 nm, the ceramics exhibit Vis UC emissions at 532 nm (green), 547 nm (green), and 660 nm (red), as well as broadband NIR and MIR DC emissions in 1.44–1.66 μm and 2.62–2.84 μm, respectively. Our results also reveal that the vacancies arisen from the charge imbalance between Er^{3+} and the replaced ions can increase the PL intensities of the NIR and MIR emissions at the expense of the visible emissions. A looping mechanism between the $^4F_{7/2}$, $^2H_{11/2}$, $^4I_{9/2}$, and $^4I_{11/2}$ levels is established in the ceramics containing V_c. As a result, the enhancement in the PL intensity of the NIR emission becomes much more significant, reaching about 70% for the BNBT-Er(Na) ceramic. The ceramics also exhibit reasonably good ferroelectric, dielectric, and piezoelectric properties, and hence they should have great potentials in multifunctional optoelectronic applications.

ACKNOWLEDGMENTS

This work was supported by the Research Grants Council of the Hong Kong Special Administrative Region (Project No. PolyU 5176/12E) and the Centre for Smart Materials of The Hong Kong Polytechnic University.

[1]F. Wang and X. Liu, Chem. Soc. Rev. **38**, 976 (2009).
[2]G. Chen, T. Y. Ohulchanskyy, A. Kachynski, H. Agren, and P. N. Prasad, ACS Nano **5**, 4981 (2011).
[3]L. Tsonev, Opt. Mater. (Amst.) **30**, 892 (2008).
[4]A. J. Silversmith, W. Lenth, and R. M. Macfarlane, Appl. Phys. Lett. **51**, 1977 (1987).
[5]S. Ivanova and F. Pellé, J. Opt. Soc. Am. B **26**, 1930 (2009).
[6]T. Sanamyan, M. Kanskar, Y. Xiao, D. Kedlaya, and M. Dubinskii, Opt. Express **19**, A1082 (2011).
[7]E. Benes, M. Groschl, W. Burger, and M. Schmid, Sens. Actuators, A **48**, 1 (1995).
[8]D. Zhou, K. H. Lam, Y. Chen, Q. Zhang, Y. C. Chiu, H. Luo, J. Dai, and H. L. W. Chan, Sens. Actuators, A **182**, 95 (2012).
[9]J. Minase, T.-F. Lu, B. Cazzolato, and S. Grainger, Precis. Eng. **34**, 692 (2010).
[10]T. Takenaka, K. Maruyama, and K. Sakata, Jpn. J. Appl. Phys., Part 1 **30**, 2236 (1991).
[11]C. Xu, D. Lin, and K. W. Kwok, Solid State Sci. **10**, 934 (2008).
[12]B. Parija, T. Badapanda, P. Sahoo, M. Kar, P. Kumar, and S. Panigrahi, Process. Appl. Ceram. **7**, 73 (2013).
[13]P. Du, L. Luo, W. Li, and Q. Yue, J. Appl. Phys. **116**, 014102 (2014).
[14]L. Luo, P. Du, W. Li, W. Tao, and H. Chen, J. Appl. Phys. **114**, 124104 (2013).
[15]Y. Zhang, J. Hao, C. L. Mak, and X. Wei, Opt. Express **19**, 1824 (2011).
[16]L. Chen, X. Wei, and X. Fu, Trans. Nonferrous Met. Soc. China **22**, 1156 (2012).
[17]M. Paredes-Olguín, I. A. Lira-Hernández, C. Gómez-Yáñez, and F. P. Espino-Cortés, Physica B **410**, 157 (2013).
[18]D. Lin and K. W. Kwok, J. Mater. Sci. **44**, 4953 (2009).
[19]P. Du, L. Luo, W. Li, Y. Zhang, and H. Chen, Mater. Sci. Eng., B **178**, 1219 (2013).
[20]Q. Lu, Q. Yang, Y. Yuan, C. Jiang, and Y. Wang, Ceram. Int. **40**, 7367 (2014).

[21]A. Yamaji, Y. Enomoto, K. Kinoshita, and T. Murakami, J. Am. Ceram. Soc. **60**, 97 (1977).
[22]M. Wu, Y. Lu, and Y. Li, J. Am. Ceram. Soc. **90**, 3642 (2007).
[23]Y. Yao, L. Luo, W. Li, J. Zhou, and F. Wang, Appl. Phys. Lett. **106**, 082906 (2015).
[24]C. M. Lau, X. Wu, and K. W. Kwok, Appl. Surf. Sci. **336**, 314 (2015).
[25]H. Sun, D. Peng, X. Wang, M. Tang, Q. Zhang, and X. Yao, J. Appl. Phys. **110**, 016102 (2011).
[26]V. E. Alexandrov, E. A. Kotomin, J. Maier, and R. A. Evarestov, Eur. Phys. J. B **72**, 53 (2009).
[27]B. Parija, T. Badapanda, V. Senthil, S. K. Rout, and S. Panigrahi, Bull. Mater. Sci. **35**, 197 (2012).
[28]S. F. Chichibu, A. Uedono, T. Onuma, B. A. Haskell, A. Chakraborty, T. Koyama, P. T. Fini, S. Keller, S. P. Denbaars, J. S. Speck, U. K. Mishra, S. Nakamura, S. Yamaguchi, S. Kamiyama, H. Amano, I. Akasaki, J. Han, and T. Sota, Nat. Mater. **5**, 810 (2006).
[29]S. F. Chichibu, A. Uedono, T. Onuma, S. P. DenBaars, U. K. Mishra, J. S. Speck, and S. Nakamura, *Advances in Light Emitting Materials* (Trans Tech Publications, 2008), pp. 233–248.
[30]G. Chai, G. Dong, J. Qiu, Q. Zhang, and Z. Yang, Sci. Rep. **3**, 1598 (2013).
[31]S.-T. Zhang, A. B. Kounga, E. Aulbach, T. Granzow, W. Jo, H.-J. Kleebe, and J. Rödel, J. Appl. Phys. **103**, 034107 (2008).